

MIT Open Access Articles

Interaction of a spark-generated bubble with a rubber beam: Numerical and experimental study

The MIT Faculty has made this article openly available. **Please share** how this access benefits you. Your story matters.

Citation: Gong, S. et al. "Interaction of a Spark-generated Bubble with a Rubber Beam: Numerical and Experimental Study." Physical Review E 86.2 (2012). ©2012 American Physical Society

As Published: <http://dx.doi.org/10.1103/PhysRevE.86.026307>

Publisher: American Physical Society

Persistent URL: <http://hdl.handle.net/1721.1/74173>

Version: Final published version: final published article, as it appeared in a journal, conference proceedings, or other formally published context

Terms of Use: Article is made available in accordance with the publisher's policy and may be subject to US copyright law. Please refer to the publisher's site for terms of use.



Interaction of a spark-generated bubble with a rubber beam: Numerical and experimental studyS. W. Gong,¹ B. H. T. Goh,² S. W. Ohl,¹ and B. C. Khoo^{3,4}¹*Institute of High Performance Computing, 1 Fusionopolis Way, #16-16, Connexis, Singapore 138632, Singapore*²*NUS Graduate School for Integrative Sciences and Engineering, 28 Medical Drive, Singapore 117456, Singapore*³*Department of Mechanical Engineering, National University of Singapore, 10 Kent Ridge Crescent, Singapore 119260, Singapore*⁴*Singapore MIT Alliance, 4 Engineering Drive 3, Singapore 117576, Singapore*

(Received 8 April 2012; revised manuscript received 3 July 2012; published 13 August 2012)

In this paper, the physical behaviors of the interaction between a spark-generated bubble and a rubber beam are studied. Both numerical and experimental approaches are employed to investigate the bubble collapse near the rubber beam (which acts as a flexible boundary) and the corresponding large deformation of the beam. Good agreement between the numerical simulations and experimental observations is achieved. The analysis reveals that the ratio of the bubble-beam distance to the maximum bubble radius influences the bubble evolution (from expansion to collapse) and the beam deformation. The stiffness of the beam plays an important role in the elastic beam response to bubble expansion and collapse. The effect of the vapor pressure on both bubble collapses and beam deflections is also examined. The results from this paper may provide physical insight into the complex physics of the bubble-rubber interaction. The understanding is possibly applicable in biomedicine for drug delivery to tissue, which is a soft material. It is also probably useful in the marine industry where ultrasonic bubbles are generated for the defouling of ship surfaces, which has been coated with an elastic material. There is also potential interest in underwater explosions near elastic structures.

DOI: [10.1103/PhysRevE.86.026307](https://doi.org/10.1103/PhysRevE.86.026307)

PACS number(s): 47.55.dd, 47.55.dp, 47.55.dr

I. INTRODUCTION

The interaction between an oscillating bubble and a flexible boundary is an important phenomenon that is commonly found in nature, marine industrial applications, and medical treatments [1]. The behavior of an oscillating bubble is greatly dependent on the characteristics of a boundary that it is placed near. If the boundary is rigid, the bubble moves towards it; whereas, if the boundary is a free surface, the bubble migrates away from it. The behavior of the bubble near a flexible boundary would fall in-between these mentioned limiting cases and is more complex.

Gibson and Blake [2] and Blake and Gibson [3] performed some of the earliest theoretical and experimental studies on the interaction between an oscillating bubble and an elastic boundary. They found that the flexibility of the boundary is crucial to the response of a nearby cavitation bubble. For an elastic boundary, they found the bubble split into smaller bubbles before collapsing with jets. Shima *et al.* [4] conducted a set of experiments of spark-generated bubbles in the vicinity of a compliant surface and observed different migratory behaviors during bubble collapse. The compliant surface has been modeled as a membrane with a spring foundation [5] or using a finite element (FE) representation [6]. Both papers found good qualitative agreement with the above experiments. Laser-induced cavitation bubbles near a flexible membrane [7], composite surface [8], elastic boundary [9,10], flat rigid surface, and flat free surface [11] were also studied. Obreschkow *et al.* [11] revealed a “microjet” enveloped by a “vapor jet” via their carefully conducted experiments and explained the jets of collapsing bubbles using their theoretical model based on the first principle.

On the other hand, complex bubble dynamics, such as splitting and mushroom-shaped collapse were observed in those spark experiments, and further understanding is reinforced

through a recent paper conducted by Turangan *et al.* [12] for the nonequilibrium bubble placed next to a (stretched) membrane. The elasticity of a membrane and the distance between the bubble and the membrane (normalized by the maximum bubble radius) remain as the two key parameters in this problem. Ohl *et al.* [13,14] conducted low-voltage spark bubble experiments and adopted a boundary element method (BEM) model to predict the dynamics of oscillating bubbles placed near a thick layer of biomaterials of different elasticities.

All the preceding papers, however, dealt with the interaction between a bubble and a thick layer, between a bubble and a very thin membrane, or between a bubble and an infinitely soft material, which can be simplified by an axial symmetry system in simulations. Moreover, the interaction between a bubble and a solid layer with other geometries, such as a slender beam remains to be explored. The present paper addresses this and investigates the physical behavior of the interaction of a spark-generated bubble and an elastic beam both numerically and experimentally. The numerical simulations were accomplished by coupling a three dimensional boundary element (BE) potential flow code with an explicit FE structural solver. The experiments were carried out using high-speed photography for the observations of the spark-generated bubble dynamics as well as the elastic beam deformation.

This paper is organized as follows. The spark-generation bubble experiment is described in Sec. II. The necessary details of the numerical methods are provided in Sec. III. The numerical and experimental results are presented in Sec. IV, which deals with the effects of the relative stand-off distance on the bubble evolution and the beam deformation, and explores the influence of the material properties on the bubble-beam interaction. Section IV also discusses the vapor pressure effect in both bubble dynamics and beam motions. Finally, Sec. V summarizes this paper.

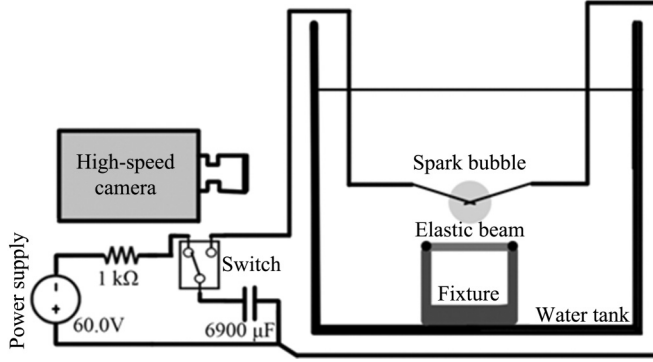


FIG. 1. Experiment setup. Experimental setup consisting of a power supply where a 6900 μF capacitor is charged to 60.0 V via a 1 k Ω resistor. The spark bubble is created in a water tank at the location of two crossed electrodes when the discharge circuit is activated with a switch. A Plexiglas fixture is placed on the bottom of the tank with screws and washers fixing a rubber beam down at its ends. The bubble dynamics are captured using a Photron Fastcam-APS RX high-speed camera.

II. EXPERIMENTS

The spark-generated bubble experimental setup used in this paper is illustrated in Fig. 1. It is composed of an electrical circuit to generate the spark bubble, a Perspex tank of dimensions 25 cm \times 25 cm \times 25 cm filled with tap water to a height of 24 cm, a high-speed imaging system, and a Perspex fixture to hold a rubber beam down at both ends. This low-voltage underwater spark-discharge method is very similar to the ones used in several other cavitation bubble investigations [12,14–18].

The electrical circuit is basically made up of a charging circuit and a discharge circuit separated by a mechanical switch. In the charging circuit, two capacitors with a total capacitance of 6900 μF are charged by a 60 V direct current power supply through a 1 k Ω resistor. The discharge circuit is composed of a pair of 0.1 mm diameter copper wires in contact and submerged under water. As soon as the capacitors are charged to 60.0 V, the discharge circuit is engaged, and a spark is created at the contact point between the electrodes. This spark turns into an oscillating vapor bubble with a maximum radius of about 5 mm in a violent process that breaks the thin electrodes. The diameter electrodes used are much smaller than the maximum bubble diameter, hence, they are believed to have a negligible effect on the system dynamics [16,17]. The contact point between the electrodes is adjusted to be at varying heights H above the centroid of a silicone rubber strip. The rubber strip has a density of 1170 kg/m³, a tensile strength of 8.34 GPa, and is supported by a Plexiglas fixture made up of two 10 mm \times 10 mm (square cross section) \times 100 mm (length) beams erected 50 mm apart and fixed down to the base of the tank (see Fig. 1). Both ends of the rubber beam are secured down onto the top of the fixture stands with stainless steel screws and 10 mm outer diameter stainless steel washers on each side. The portion of the rubber beam suspended has dimensions of 50 mm (L) \times 10 mm (W) \times 1.5 mm (H). The top surface of the rubber beam is 120 mm above the floor of the

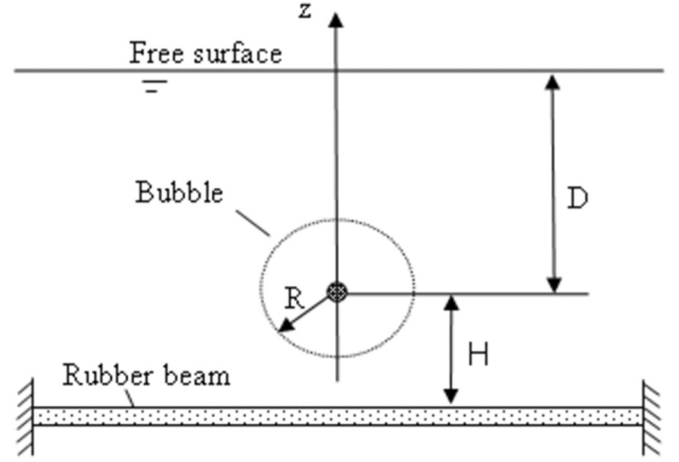


FIG. 2. A schematic showing the configuration of a nonequilibrium bubble and a rubber beam. A Cartesian coordinate system O_{xyz} is used with the z axis pointing in the opposite direction of gravity, and its origin is at the center of the upper surface of the beam. R is the bubble radius, H is the distance of the bubble center to the upper surface of the beam, and D is the bubble center to the free surface on top. Note that, in all cases studied, the free surface is very far away and is deemed not to be influencing the bubble dynamics.

tank when at rest, and the spark bubble is created at a height H of up to 20 mm for this paper.

All experiments are performed under atmospheric pressure and at room temperature (24 $^{\circ}\text{C}$). A Photron Fastcam-APX RS high-speed camera is used at 20 000 fps, and a shutter speed of 1/40 000 s is used to capture the dynamics of the problem. Viscosity effects remain negligible in this paper due to the relatively large size of the bubbles [19]. Surface tension effects are also unimportant as the Weber number for an oscillating bubble in water is on the order of 10^3 [20,21].

III. NUMERICAL METHODS

A model that described the interaction between a spark-generated bubble and a rubber beam is considered as shown in Fig. 2. The bubble has a distance H from its initial center to the upper surface of the rubber beam. A Cartesian coordinate system O_{xyz} is used with the z axis pointing in the opposite direction of gravity. The bubble dynamics near the beam are simulated based on the numerical procedure detailed in Ref. [22]. After the receding shock wave, the subsequent flow dynamics surrounding the initial bubble are practically driven by fluid inertia. At this stage, it is assumed that the fluid is inviscid and incompressible, and therefore, a velocity potential that satisfies Laplace's equation ($\nabla^2 \Phi = 0$) applies [22]. Let V_0 and p_0 denote the initial volume and pressure at the time of inception of the bubble; the pressure inside the bubble is supposed to be spatially uniform and is updated adiabatically from the ratio of the volume $p_b = p_0(V_0/V)^\gamma$. The time-dependent Bernoulli equations can be applied. On the bubble surface,

$$\rho \frac{\partial \Phi}{\partial t} = p_{\text{ref}} - p_v - p_0 \left(\frac{V_0}{V} \right)^\gamma - \frac{1}{2} \rho |\vec{u}|^2 - \rho g z, \quad (1)$$

and on the wet surface of the structure,

$$\rho \frac{\partial \Phi}{\partial t} = p_{\text{ref}} - \frac{1}{2} \rho |\vec{u}|^2 - \rho g z - p_s, \quad (2)$$

where Φ is a velocity potential that obeys the relation for the velocity vector $\vec{u} = \nabla \Phi$, ρ is the density of the fluid, g is the gravity acceleration, p_{ref} and p_v are the reference pressure and vapor pressure, and p_s is the pressure of the fluid in contact with the wet surface of the structure.

Numerically, Eqs. (1) and (2) can be solved for Φ if the initial conditions, which initiate the bubble, are known. However, in practice, the initial conditions are not always available for use. Since it is difficult to correlate the discharge energy of the circuit to the initial conditions of the spark bubble, we propose using a small equivalent charge weight W to determine the initial conditions of the spark bubble with reference to the scaling law for different bubbles [23]. This is based on the principle that the potential energy E (converted from the electric spark) for a bubble to reach its maximum volume is similar to the potential energy E (converted from the underwater expulsion) for the bubble to reach the same maximum volume as the spark-generated bubble.

We can estimate the maximum radius of a bubble induced by an underwater explosion in terms of the charge weight W [23],

$$R_m = \left(\frac{3K_{EW}}{4\pi\rho g} \right)^{1/3} \times \frac{W^{1/3}}{\left(D + \frac{p_{\text{ref}} - p_v}{\rho g} \right)^{1/3}}. \quad (3)$$

Here, D is the water depth of the charge, K_{EW} represents the potential energy E per charge weight W ($K_{EW} = E/W$). The coefficient K_{EW} in $(\text{m/s})^2$ is a measure of energy effectiveness of an explosive charge and can be obtained from underwater explosive tests for different types of charges. Let $K_R = (3K_{EW}/4\pi\rho g)^{1/3}$; we can then get the value of $K_R = 3.36 \text{ m}^{4/3} \text{ kg}^{-1/3}$ for a trinitrotoluene (TNT) charge [24,25]. For a spark-generated bubble with a prescribed maximum radius R_m , the small equivalent charge weight W (that produces the bubble with the same maximum radius R_m) can be determined by

$$W = \left(D + \frac{p_{\text{ref}} - p_v}{\rho g} \right) \left(\frac{R_m}{K_R} \right)^3. \quad (4)$$

With the prescribed maximum bubble radius R_m and the small equivalent charge weight W , we can proceed to find the initial conditions for the simulation of the spark-generated bubble. Assume the bubble to be spherical at the beginning of the numerical calculations, and the initial bubble radius R_0 (or $V_0 = 4\pi R_0^3/3$) can be obtained from the following equation by using a root solving procedure [22]:

$$\begin{aligned} & (p_{\text{ref}} - p_v + \rho g D) \left[-1 + \left(\frac{R_0}{R_m} \right)^3 \right] \\ &= \frac{1.39 \times 10^5}{\gamma - 1} \left(\frac{3W}{4\pi R_0^3} \right)^\gamma \left[\left(\frac{R_0}{R_m} \right)^{3\gamma} - \left(\frac{R_0}{R_m} \right)^3 \right], \end{aligned} \quad (5)$$

and p_0 can be related to the charge weight by the empirical equation [24],

$$p_0 = 1.39 \times 10^5 \left(\frac{W}{V_0} \right)^\gamma, \quad (6)$$

and the ratio of the specific heats γ equals 1.25 for a TNT charge. With the initial conditions V_0 and p_0 , Eqs. (1) and (2) can be solved for Φ , which enables the simulation of bubble behavior and the prediction of the pressure anywhere in the fluid via a BEM.

The dynamics of the rubber beam in response to the nearby bubble is simulated via the finite element method (FEM). The material model proposed by Blatz and Ko for rubber [26] is employed for this paper in which the strain energy density function can be expressed as [26]

$$\begin{aligned} W = \frac{G}{2} & \left\{ f(J_1 - 3) + (1 - f)(J_2 - 3) + \left(\frac{1 - 2\nu}{\nu} \right) \right. \\ & \left. \times [f(J_3^{-2\nu/(1-2\nu)} - 1) + (1 - f)(J_3^{2\nu/(1-2\nu)} - 1)] \right\}. \end{aligned} \quad (7)$$

In Eq. (7), G , ν , and f are the material constants; J_1 , J_2 , and J_3 are the invariants defined as $J_1 = \lambda_1^2 + \lambda_2^2 + \lambda_3^2$, $J_2 = 1/\lambda_1^2 + 1/\lambda_2^2 + 1/\lambda_3^2$, and $J_3 = \lambda_1\lambda_2\lambda_3$, where λ_1 , λ_2 , and λ_3 are the principal stretch ratios of the deformation at the point considered. Note that, as $J_3 = 1$, Eq. (7) becomes the well-known Mooney-Rivlin strain-energy density for incompressible materials [27]. Furthermore, the special case, which assumes $J_3 = 1$ and $f = 1$ in Eq. (7), may be reviewed as the neo-Hookean incompressible material [27]. Blatz and Ko suggested using $f = 1$ and $J_3 \neq 0$ based on their experiments [26], which is appropriate for solid rubber provided the extension is less than about 200%. The strain energy (7) then can be simplified to [26]

$$W = \frac{G}{2} \left[(J_1 - 3) + \left(\frac{1 - 2\nu}{\nu} \right) (J_3^{-2\nu/(1-2\nu)} - 1) \right]. \quad (8)$$

We calculate the spark-generated bubble using a potential flow code based on the BEM [22,28–31] and compute the structural response of the rubber beam to bubble pressure using an explicit solver based on the FEM with the implementation of the material constitutive equations for the rubber material [32]. The interaction of the bubble and the elastic beam is simulated via the coupling between the BE code and the FE solver. In the coupling computation, the pressure at the interface (or wet surface of the beam) in a fluid domain induced by the nonequilibrium bubble is calculated using the BE code, and it is then given as inputs to the FE solver. The FE solver then calculates the displacements of the rubber beam, which are then returned as inputs for the fluid BE code.

In the view that a beam's response to an external pressure in air differed from the beam in its response to the same pressure in water and the Blatz and Ko model was employed for a rubber material with the FE solver [32], an added mass was included in the FE solver accordingly [32] in the simulation for the beam in response to the pressure induced by bubble oscillations. In a physical sense, this added mass is the weight added to the beam due to the acceleration or deceleration of the beam. It must move some volume of surrounding fluid with it as it moves. For the rectangular cross section of the beam, the added mass was estimated by [33,34] $m_{\text{add}} = \alpha\pi\rho b^2$, where α is the coefficient depending on the ratio of the width to the thickness at the cross section; it ranges from 1.21 to 1.14, corresponding to a ratio of b/h from 5 to 10 [33,34].

IV. RESULTS AND DISCUSSIONS

A. Bubble collapse at different $H' = H/R_m$

The collapses of the spark-generated bubbles near the rubber beam were recorded experimentally and were calculated using the coupled BEM and FEM codes. In this paper, three relative standoff distances ($H' = H/R_m$) were considered: $H' = 0.97$, $H' = 1.38$, and $H' = 3.10$. For the purpose of comparison, the beam has the same size, the same material parameters, and the same boundary conditions as those described in the above experiment. The density of the fluid, the reference pressure, and the vapor pressure [12] are assumed to be 1000 kg/m^3 , 0.1 , and 0.5 MPa , respectively.

To simulate bubble behavior and to predict the pressure anywhere in the fluid, the equivalent small charges of TNT were estimated by Eq. (4) with the prescribed maximum radius

TABLE I. The three sets of input parameters for the simulations, which are derived from the experiments. R_m is the maximum radius of the bubble, and W is the weight, in grams, of the explosive TNT.

Case	H'	R_m (mm)	W (g)
1	0.97	4.64	2.7×10^{-5}
2	1.38	4.76	2.8×10^{-5}
3	3.10	4.64	2.7×10^{-5}

R_m that matches the bubble from the experiments. With the equivalent small charges of TNT, the initial data of V_0 and p_0 can be obtained using Eqs. (5) and (6) accordingly, which enables the simulation of bubble behavior and the prediction of the pressure anywhere in the fluid by solving Eqs. (1) and (2). The initial bubble radius R_0 and the initial pressure P_0 used in the simulations are $R_0 = 0.157 R_m$ and $p_0 = 44.3 p_{\text{ref}}$.

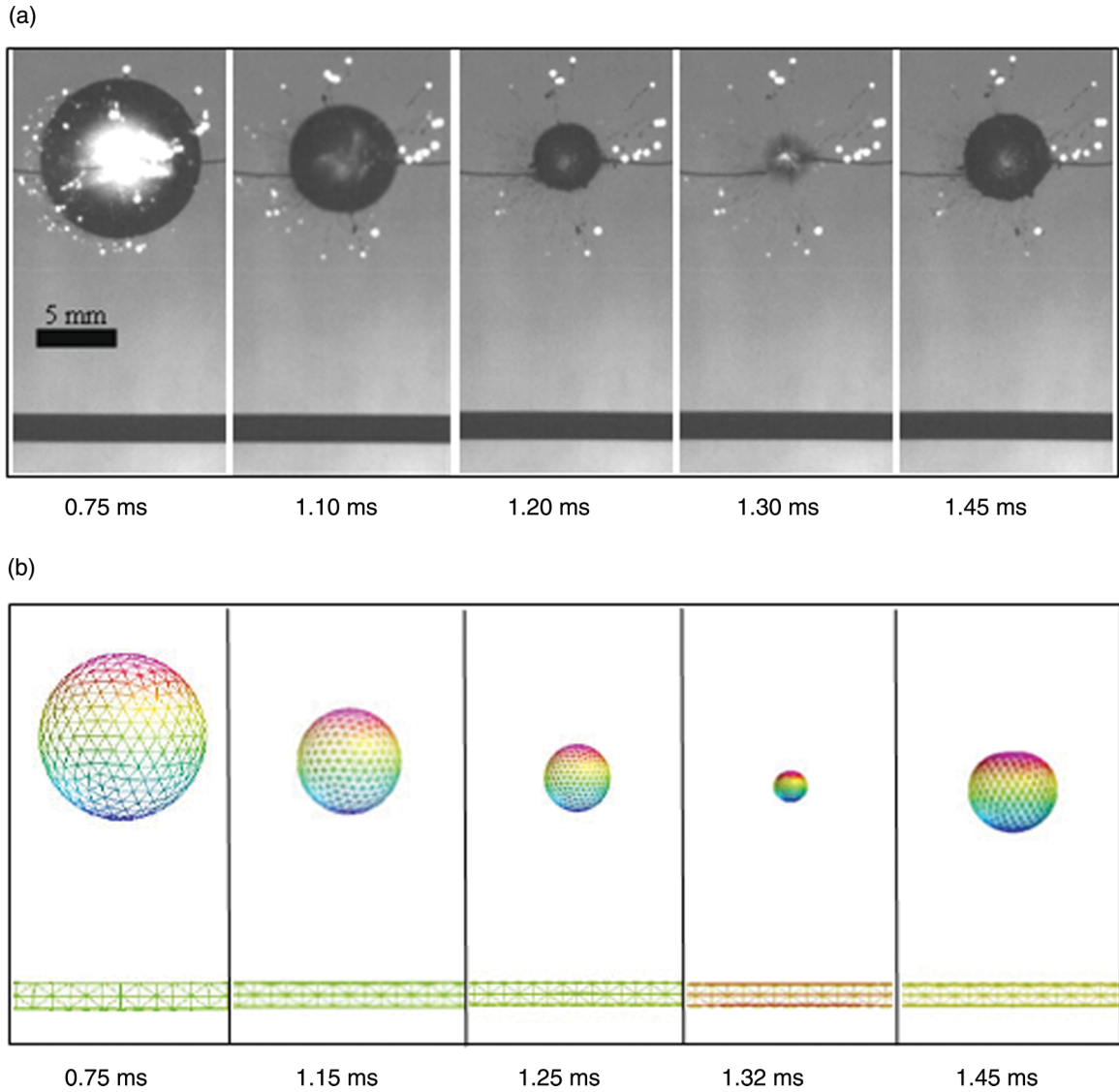


FIG. 3. (Color online) Collapse phase of the spark bubble, which is initiated very far ($H' = 3.18$) from the rubber beam. The scale bar is given in the first frame. The times for each frame are 0.75, 1.1, 1.2, 1.3, 1.45 ms from the first spark observed (which is taken to be time = 0.0 ms then). The bubble grows from 0.0 ms to its maximum size of $R_m = 4.64 \text{ mm}$ at 0.75 ms. It is observed that the bubble collapses spherically (frames 1–4) and then rebounds (frame 5). The rubber beam below hardly moves. (a) Experimental results, (b) numerical results.

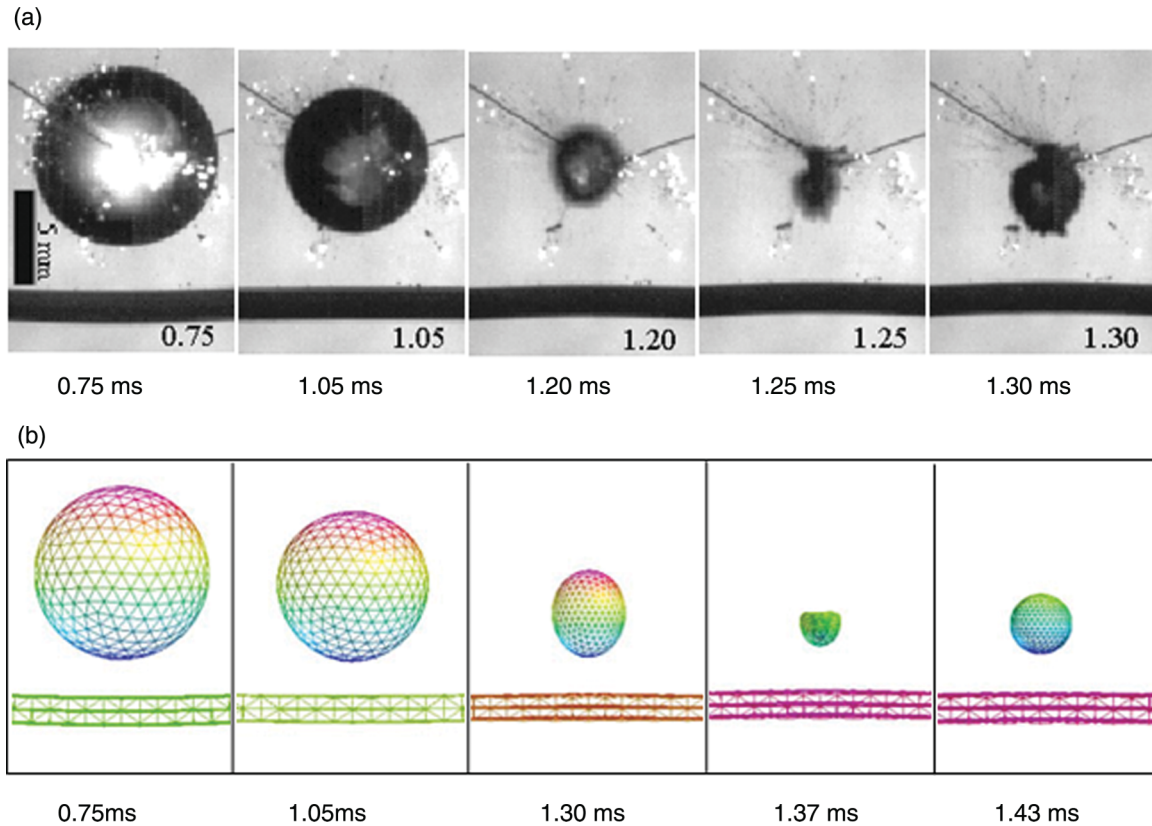


FIG. 4. (Color online) Collapse phase of the spark bubble at $H' = 1.38$ from the rubber beam. The scale bar is given in the first frame. The times for each frame (in milliseconds) are as indicated. The bubble grows from 0.0 ms to its maximum size of $R_m = 4.76$ mm at 0.75 ms. Thereafter, the bubble contracts with a jet towards the beam as it collapses, and the beam moves slightly towards the bubble. The bubble reexpands after 1.30 ms. (a) Experimental results with the bubble collapsing at 1.25 ms. (b) Numerical results with the bubble collapsing at 1.37 ms.

The estimated charge weights of TNT and the corresponding maximum radii of the bubbles are listed in Table I.

Figure 3 shows the collapse phase of the spark bubble, which is initiated very far ($H' = 3.18$) from the rubber beam. The time sequences shown for each frame are 0.75, 1.1, 1.2, 1.3, 1.45 ms from the first spark observed (which is taken to be time = 0.0 ms then). The simulation results match well with the experimental results for all the time frames. The bubble grows from 0.0 ms to its maximum size of $R_m = 4.64$ mm at 0.75 ms. It is observed that the bubble collapses spherically (frames 1–4) and then rebounds (frame 5).

Figure 4 shows the collapse phase of the spark bubble at $H' = 1.38$ from the rubber beam. The bubble grows from 0.0 ms to its maximum size of $R_m = 4.76$ mm at 0.75 ms. Thereafter, the bubble collapses with a jet towards the beam, and the beam moves slightly towards the bubble. The bubble reexpands after 1.25 ms. The experimental spark bubble collapses at 1.25 ms, whereas, the numerical bubble collapses at 1.37 ms. It is interesting to note that the upward deflection of the beam in response to the bubble collapse is shown in both the experiment and the simulation.

Figure 5 explores the case of the spark bubble created near the rubber beam with $H' = 0.97$. The bubble grows from 0.0 ms to its maximum size of $R_m = 4.64$ mm at 0.75 ms. The bubble expansion causes the beam to deform downwards. From 0.95 ms, the bubble contracts nonspherically. The

bubble bottom is flattened, and it forms an elongated shape. Experimental results show the bubble collapsing at 1.25 ms, whereas, in numerical simulation, the bubble contracts with a slightly longer time, collapsing at 1.36 ms. The longer collapse time predicted in the simulations for cases 2 (Fig. 4) and 3 (Fig. 5) might arise from a higher vapor pressure (0.5 bar) assumed in the simulation, which may retard the bubble collapse. The actual vapor pressure in the spark bubble, however, cannot be measured easily. From the previous papers [12,17], we estimate it to be between 0.3 and 0.7 bar. The variation could be due to the fact that the electrodes are wound around the wires and that they have to be replaced after several sets of experiments. The tightness of the winding as well as the contact area of the electrodes seems to have some influence on the vapor pressure (estimated from the bubble's collapse time).

From the second last image of Fig 5, it is also observed that the lower part of the numerical bubble does not fit so well with the experimental spark bubble. There is a counterjet in the experiment, which could be due to the shock wave reflected from the surface. This is not modeled in the simulation. Another plausible reason may be that, in the simulation, the pressure (including vapor pressure) inside the bubble is assumed to be uniformly distributed at each time instant, whereas, the pressure (including vapor pressure) in the experimental spark bubble is unlikely to be

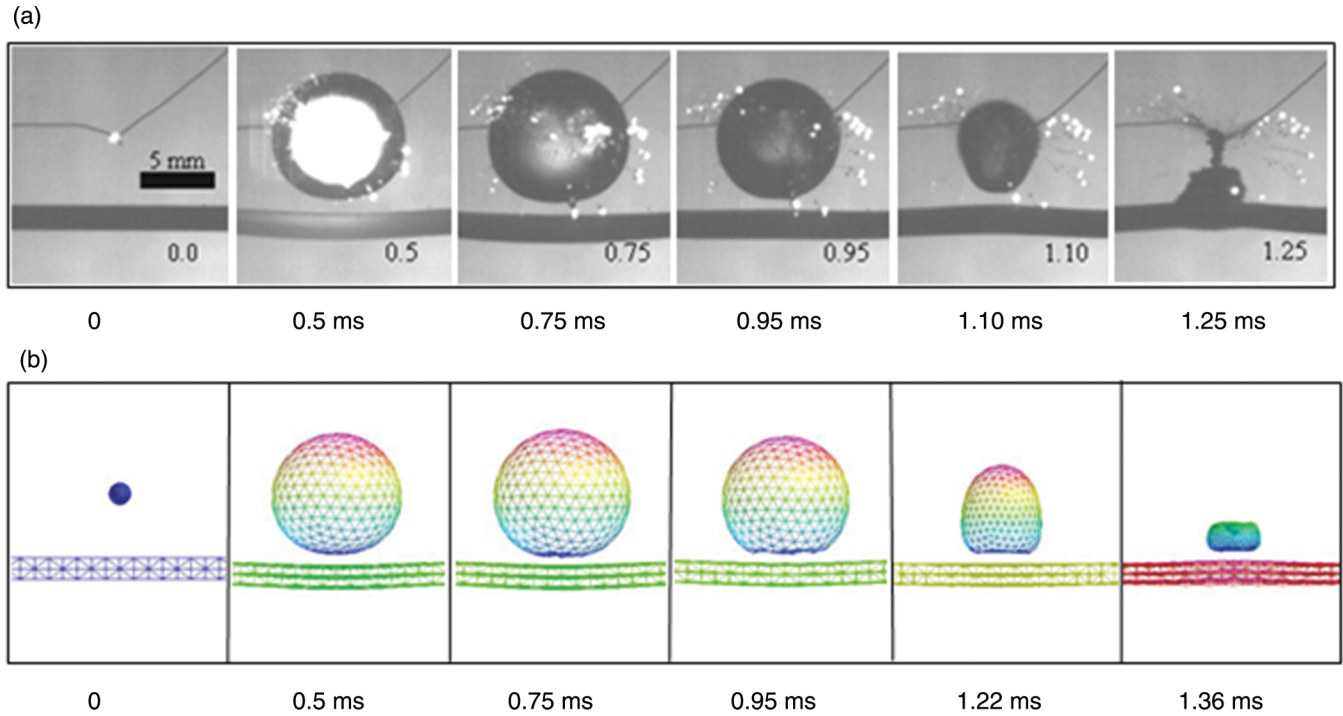


FIG. 5. (Color online) The spark bubble nearer ($H' = 0.97$) to the rubber beam. The scale bar is given in the first frame. The times for each frame (in milliseconds) are as indicated. The bubble grows from 0.0 ms to its maximum size of $R_m = 4.64$ mm at 0.75 ms. The bubble expansion causes the beam to deform downwards. From 0.95 ms, the bubble contracts nonspherically. The bubble bottom is flattened, and it forms an elongated shape. (a) Experimental results with the bubble collapsing at 1.25 ms. (b) Numerical results with the bubble collapsing at 1.36 ms.

(almost) instantaneously uniform, especially when the bubble is collapsing violently near the beam.

An overview of the above three cases for all the time frames, however, shows that the simulation results for bubble evolution match reasonably with the experimental results, although there still is room for improving the simulation if we could estimate the pressure inside the bubble with higher accuracy. This could be part of our future work.

B. The beam with different materials in response to bubble evolution

The deflection of the rubber beam induced by the spark-generated bubble was also investigated numerically and experimentally. Table II lists the beam maximum deflections predicted from the simulation and measured from the experiment, respectively. The simulation results match reasonably

with the experimental data, which attest that the present simulation is fairly effective.

We extended the simulations to the beam with different materials in response to the bubble evolution at $H' = 0.97$. In the previous paper [13], several aspects of a bubble oscillating near different biomaterials were explored. In this paper, we placed much emphasis on the response of the biomaterials to bubble oscillation. This is because a nonequilibrium bubble can be made to oscillate and to collapse in the vicinity of nearby tissues or organs in some medical procedures [13]. Furthermore, the behavior of the tissues or organs in response to the bubble oscillation will, in turn, influence the success of the clinical procedures, and the collateral damages, if any, will be borne by the patients. For more details on the type of medical situations where an oscillating bubble might occur next to biomaterials, the reader is encouraged to refer to Ref. [13]. In general, when ultrasound, shock waves, or laser systems are used for medical treatment, it is possible that cavitation

TABLE II. Experiment and simulation comparisons for central deflections of the rubber beam.

Case	H'	Mix deflections (downwards)		Mix deflections (upwards)	
		Expt. z (mm) ^a	Sim. z (mm)	Expt. z (mm) ^a	Sim. z (mm)
1	0.97	−0.641	−0.607	0.214	0.217
2	1.38	−0.435	−0.421	0.174	0.212
3	3.10	−0.171	−0.150	~0.00	0.021

^aThe z axis points in the opposite direction of the gravitational acceleration vector.

TABLE III. The parameters used in the simulation for various materials.

Material	Density (kg/m ³)	Young's modulus (kPa)	Poisson ratio
Muscle	1060	790	0.45
Rubber	1190	2350	0.46
Cartilage	1300	5000	0.4
Cervical bone	3000	7300	0.22

bubbles may form within the bodily fluid, e.g., in an ultrasonic liposuction procedure (an oscillating bubble near fat tissue) and others. This paper can also be regarded as an extension of the previous paper [13] in which the bubble behaviors near the different biomaterials were explored extensively.

Table III lists the parameters of the materials, which are taken from Refs. [13,35,36]. The parameters of the rubber material [35] fall in-between the muscle and the cartilage [13], which are regarded as soft biomaterials. Figure 6 shows the central deflection of the beam z_{bc} for four different materials. The maximum downward deflection increases as the beam stiffness (or Young's modulus) decreases. The beam with the muscle material exhibits the largest deflection when the bubble reaches its maximum radius. The maximum upward deflection decreases as the beam stiffness (or Young's modulus) decreases when the bubble collapses. This may be explained by the fact that more energy is needed to revert the beam to its original state for the softer material, such as the muscle, and furthermore, the bubble jet would be away from the surface of the beam as its material becomes softer. A higher value of the maximum upward deflection for the beam with the cartilage is also observed; this may be explained by the fact that the density of the beam with the cartilage is lower than the density of the beam with the cervical bone.

Figure 7 shows the distribution of the internal energy over the beams with various materials when a bubble collapses at $t = 1.39$ ms. It is observed that the energy distributes locally around the center of the beams and attenuates outward to the beam ends. The beam with the muscle material gains the

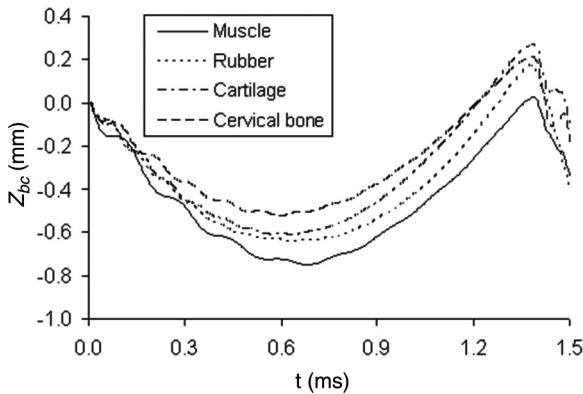


FIG. 6. Time histories of the central deflection z_{bc} of the beam for four different materials: solid line: muscle; dotted line: rubber; dashed-dotted line: cartilage; and dashed line: cervical bone. The maximum downward deflection increases as the beam stiffness decreases, reaching the maximum around $t = 0.7$ ms for all cases.

Energy density (J/kg)

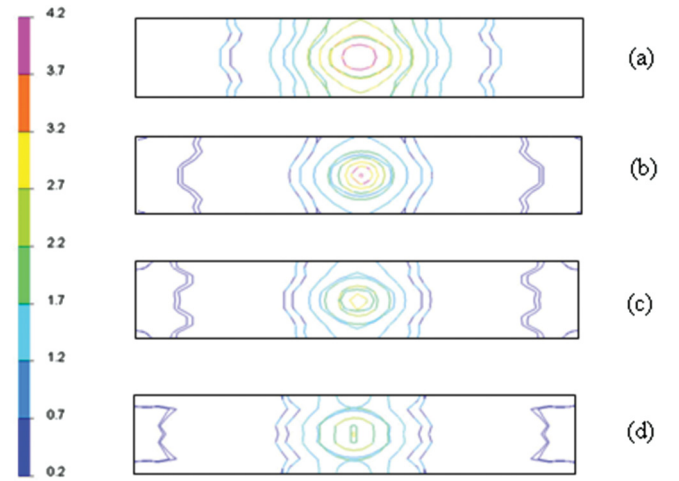


FIG. 7. (Color online) The distribution of the internal energy over the beams with various materials at $t = 1.39$ ms. (a) Beam with muscle material. (b) Beam with rubber material. (c) Beam with cartilage material. (d) Beam with bone material.

highest energy and shows the lowest energy at the two ends on being compared with the beams of the other materials. The energy distribution pattern of the beam with the rubber material is close to the beam with the cartilage material, hence, indicating that the rubber material would be a potential substitute for the soft biomaterials.

C. Effect of vapor pressure

When an electrical spark generates a bubble, the energy deposited at the electrodes is initially stored in a high temperature and high pressure plasma. It is found to have a rather high vapor pressure [12,15], which is difficult to measure in the experiments. However, it is possible to estimate the vapor pressure based on a curve fitting of the numerical results with the experimental observations. Buogo and Cannelli [15] found that, in their experiment on a spark-generated bubble, the vapor pressure varied with the temperature; it reached 0.3 bar corresponding to a vapor temperature of 69 °C.

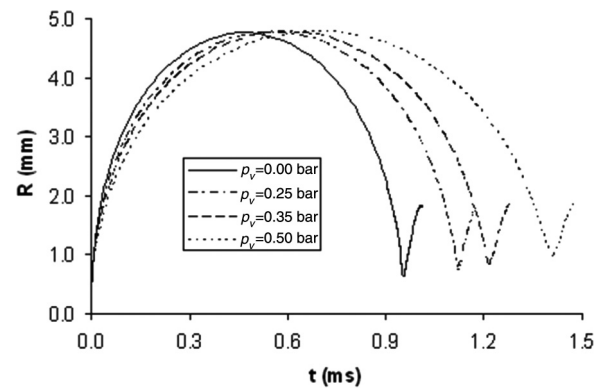


FIG. 8. The bubble radius-time histories for various vapor pressures: solid line: $p_v = 0$ bar; dashed-dotted line: $p_v = 0.25$ bar; dashed line: $p_v = 0.35$ bar; and dotted line: $p_v = 0.50$ bar.

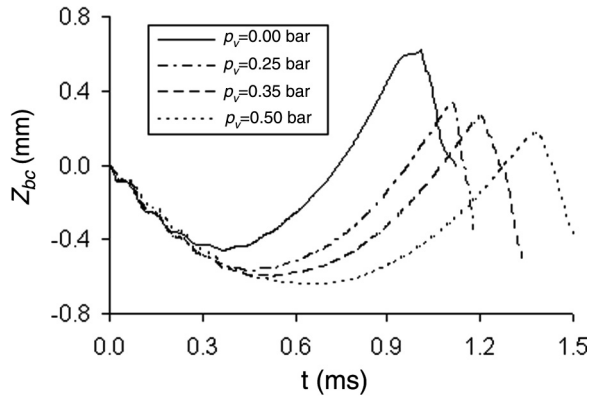


FIG. 9. Time histories of the central deflection z_{bc} of the beam for various vapor pressures: solid line: $p_v = 0$ bar; dashed-dotted line: $p_v = 0.25$; dashed line: $p_v = 0.35$ bar; and dotted line: $p_v = 0.50$ bar. The central deflection of the beam reduces as the vapor pressure increases with its maximum value occurring sequentially.

Turangan *et al.* [12] found that, with a higher vapor pressure of $p_v = 0.5$ bar, the bubble radius-time curve from their simulations matched well with their experimental results.

Figure 8 shows the bubble radius-time histories for various vapor pressures in our simulations. The bubble reaches its maximum radius and collapses at different times with the different vapor pressures. The period of the bubble increases as the vapor pressure increases. As a result, the beam, in response to bubble collapse, varies with the vapor pressure as shown in Fig. 9. The central deflection of the beam is reduced as the vapor pressure increases. The time instant at which the beam deflection reaches its maximum value is also delayed as the vapor pressure becomes higher. This appears reasonable since a higher vapor pressure may dissipate more energy. A proper estimation of the vapor pressure may come from curve fitting of the radius-time histories from experiments and

simulations, respectively, which may range from 0 to 0.5 bar ($0 \text{ bar} < p_v \leq 0.5 \text{ bar}$).

V. CONCLUSION

We have studied the interaction of a spark-generated bubble with a rubber beam via both simulations and experiments. The experimental setup for spark-generated bubbles was described, and three selected experimental cases were compared with the simulations employing the coupled BE potential flow code and FE structural solver. The simulations reasonably described the bubble dynamic (or bubble growth and collapse), the rubber-beam deflections, and the behavior of the bubble-rubber-beam interaction. The parametric study illustrated the significant influence of the rubber beam on the bubble evolution at $H' \leq 1$. Exploring the interaction between the spark bubble and the beam with different materials showed that the beam with softer material experienced the larger deflection when the bubble reached its maximum radius and also gained the higher energy at the bubble's collapse. The simulation results also demonstrated that the vapor pressure retarded the bubble collapse and, thus, influenced the deflection of the beam. From the curve fitting of the radius-time histories from experiments and simulations, respectively, the vapor pressure in a spark bubble could be estimated, and it ranges from 0 to 0.5 bar.

In a future paper, the simulation method for the prediction of the vapor pressure in the bubble with higher accuracy to accommodate its variation in a bubble collapse will be explored.

ACKNOWLEDGMENTS

The authors thank the National University of Singapore's Impact Mechanics Laboratory for their help and support for the spark-generated bubble test. The authors also thank Dr. E. Klaseboer for the helpful discussions on bubble dynamics and numerical methods.

-
- [1] W. Lauterborn and T. Kurz, *Rep. Prog. Phys.* **73**, 106501 (2010)
 - [2] D. C. Gibson and J. R. Blake, *Appl. Sci. Res.* **38**, 215 (1982).
 - [3] J. R. Blake and D. C. Gibson, *Annu. Rev. Fluid Mech.* **19**, 99 (1987).
 - [4] A. Shima, Y. Tomita, D. C. Gibson, and J. R. Blake, *J. Fluid Mech.* **203**, 199 (1989).
 - [5] J. H. Duncan and S. Zhang, *J. Fluid Mech.* **226**, 401 (1991).
 - [6] J. H. Duncan, C. D. Milligan, and S. Zhang, *J. Sound Vib.* **197**, 17 (1996).
 - [7] S. J. Shaw, Y. H. Jin, T. P. Gentry, and D. C. Emmony, *Phys. Fluids* **11**, 2437 (1999).
 - [8] Y. Tomita and T. Kodama, *J. Appl. Phys.* **94**, 2809 (2003).
 - [9] E. A. Brujan, K. Nahen, P. Schmidt, and A. Vogel, *J. Fluid Mech.* **433**, 251 (2001).
 - [10] E. A. Brujan, K. Nahen, P. Schmidt, and A. Vogel, *J. Fluid Mech.* **433**, 283 (2001).
 - [11] D. Obreschkow, M. Tinguely, N. Dorsaz, P. Kobel, A. de Bosset, and M. Farhat, *Phys. Rev. Lett.* **107**, 204501 (2011).
 - [12] C. K. Turangan, G. P. Ong, E. Klaseboer, and B. C. Khoo, *J. Appl. Phys.* **100**, 054910 (2006).
 - [13] S. W. Ohl, E. Klaseboer, and B. C. Khoo, *Phys. Med. Biol.* **54**, 6313 (2009).
 - [14] S. W. Ohl, E. Klaseboer, and B. C. Khoo, *Mod. Phys. Lett. B* **24**, 1365 (2010).
 - [15] S. Buogo and G. B. Cannelli, *J. Acoust. Soc. Am.* **111**, 2594 (2002).
 - [16] K. S. F. Lew, E. Klaseboer, and B. C. Khoo, *Sens. Actuators, A* **133**, 161 (2007).
 - [17] S. W. Fong, D. Adhikari, E. Klaseboer, and B. C. Khoo, *Exp. Fluids* **46**, 705 (2009).
 - [18] A. Pain, B. H. T. Goh, E. Klaseboer, S.-W. Ohl, and B. C. Khoo, *J. Appl. Phys.* **111**, 054912 (2012).
 - [19] M. Versluis, D. E. Goertz, P. Palanchon, I. L. Heitman, S. M. van der Meer, B. Dollet, N. de Jong, and D. Lohse, *Phys. Rev. E* **82**, 026321 (2010).
 - [20] S. Rungsiyaphornrat, E. Klaseboer, B. C. Khoo, and K. S. Yeo, *Comput. Fluids* **32**, 1049 (2003).

- [21] Z. Y. Zhang and H. S. Zhang, *Phys. Rev. E* **71**, 066302 (2005).
- [22] E. Klaseboer, K. C. Hung, C. Wang, C. W. Wang, B. C. Khoo, P. Boyce, S. Debono and H. J. Charlier, *J. Fluid Mech.* **537**, 387 (2005).
- [23] S.W. Gong, S. W. Ohl, E. Klaseboer, and B. C. Khoo, *Phys. Rev. E* **81**, 056317 (2010).
- [24] R. H. Cole, *Underwater Explosions* (Princeton University Press, Princeton, 1948).
- [25] E. Swift and J. C. Decius, *Underwater Explosion Research* (Office of Naval Research, Washington D.C., 1950), Vol. II.
- [26] P. J. Blatz and W. L. Ko, *Soc. Rheol. Trans.* **6**, 223 (1962).
- [27] C. O. Horgan, *J. Elast.* **42**, 165 (1996).
- [28] Q. X. Wang, K. S. Yeo, B. C. Khoo, and K. Y. Lam, *Comput. Fluids* **25**, 607 (1996).
- [29] Y. L. Zhang, K. S. Yeo, B. C. Khoo, and W. K. Chong, *J. Comput. Phys.* **146**, 105 (1998).
- [30] Y. L. Zhang, K. S. Yeo, B. C. Khoo, and C. Wang, *J. Comput. Phys.* **166**, 336 (2001).
- [31] C. Wang, B. C. Khoo, and K. S. Yeo, *Comput. Fluids* **32**, 1195 (2003).
- [32] PAM-CRASH, *Solver Reference Manual* (Pam System International, Paris, 2002).
- [33] C. E. Brennen, Naval Civil Engineering Laboratory Report No. CR82.010, 1982 (unpublished).
- [34] C. E. Brennen, *Cavitation and Bubble Dynamics* (Oxford University Press, New York, 1995).
- [35] J. M. Gere and S. P. Timoshenko, *Mechanics of Materials* (PWS, Boston, 1984).
- [36] J. S. Ruan, T. B. Khalil, and A. I. King, *J. Biomech. Eng.* **116**, 44 (1994).